Genetic Differentiation and Divergence Time of Chinese *Parnassius* (Lepidoptera: Papilionidae) Species Based on Nuclear Internal Transcribed Spacer (*ITS*) Sequence Data[1]

Chengcai Si, Keke Chen, Ruisong Tao, Chengyong Su, Junye Ma[3], Luyan Li[3], Jiasheng Hao[2], and Qun Yang[2,3,4]

Laboratory of Molecular Evolution and Biodiversity, College of Life Sciences, Anhui Normal University, Wuhu 241000, China

J. Entomol. Sci. 55(4): 520–546 (October 2020)

Abstract *Parnassius* (Lepidoptera: Papilionidae) is a genus of attractive butterflies mainly distributed in the mountainous areas of Central Asia, the Himalayas, and western China. In this study, we used the internal transcribed spacer (*ITS1* and *ITS2*) sequence data as DNA barcodes to characterize the genetic differentiation and conduct the phylogenetic analysis and divergence time estimation of the 17 *Parnassius* species collected in China. Species identification and genetic differentiation analysis suggest that the *ITS* barcode is an effective marker for *Parnassius* species identification; additionally, a relatively high level of genetic diversity and low level of gene flow were detected in the five *Parnassius* species with diverse geographic populations. Phylogenetic analysis indicates that the 17 species studied were clustered in six clades (subgenera), with subgenus *Parnassius* at the basal position in the phylogenetic trees. Bayesian divergence time estimation shows that the genus originated about 18 million years ago during the early Miocene, correlated with orogenic events in the distribution region, probably southwestern China about 20–10 million years ago. Our estimated phylochronology also suggests that the *Parnassius* interspecific and intraspecific divergences were probably related with the rapid rising of the Qinghai-Tibet Plateau, the Tibet Movement, the Kunlun-Yellow River Tectonic Movement, and global cooling associated with intensified glaciation in the region during the Quaternary Period.

Key Words *Parnassius*, genetic differentiation, phylogeny, divergence time estimation, *ITS* DNA barcode

The *Parnassius* are one of the most charming butterfly groups of subfamily Parnassiinae within family Papilionidae, often called "Apollos." Species in the genus, totaling about 60 worldwide, are distributed mostly in high-altitude mountainous areas of the Himalayas, Central Asia, western China, and other parts of northern Eurasia (Condamine 2018, Katoh et al. 2005, Omoto et al. 2009), with 33 species reported in China (Chou 1999). Several recent attempts to resolve the

[1]Received 20 November 2019; accepted for publication 22 December 2019.
[2]Corresponding authors: J. Hao (email: jshaonigpas@sina.com) and Q. Yang (email: qunyang@nigpas.ac.cn).
[3]State Key Laboratory of Palaeontology and Stratigraphy, Nanjing Institute of Geology and Paleontology, Center for Excellence in Life and Paleoenvironment, Chinese Academy of Sciences, Nanjing 210008, China.
[4]College of Earth and Planetary Sciences, University of Chinese Academy of Sciences, Beijing 100049, China.

phylogenetic relationships within *Parnassius* based on molecular and morphological data sets have provided considerable resolutions, but some intersubgeneric relationships have not been well supported while others were mutually contradicted among studies (Condamine et al. 2013, 2018b; Katoh et al. 2005; Michel et al. 2008; Omoto et al. 2004; Zheng et al. 2018). For example, Omoto et al. (2004) used the analysis of mitochondrial *ND5* gene to propose the division of eight subgenera. Michel et al. (2008) obtained similar results based on four mitochondrial DNA segments (*COI*, *ND1*, *ND5*, *16S rRNA*), and named these eight subgenera (*Parnassius*, *Kailasius*, *Koramius*, *Kreizbergia*, *Lingamius*, *Driopa*, *Sachaia*, and *Tadumia*); however, Katoh et al. (2005) and Zheng et al. (2018) acquired different results about the subgeneric relations, based on mitochondrial genes. Additionally, contradictory results were reported by Condamine et al. (2013) and Condamine et al. (2018b) using similar criteria.

The elevation of the Qinghai-Tibet Plateau experienced dramatic uplift during the frequent orogeny of the Cenozoic epoch, and its southern part likely reached an elevation comparable to present-day elevation during the Miocene, transforming the local environments, as well as causing the aridification of Central Asia (Du et al. 2019, Favre et al. 2015, Najman et al. 2010), and its high-elevation environments also experienced dramatic physical changes during the cyclical expansion and retreat of glacial ice sheets in the Quaternary (Shi 2002, Xu et al. 2010, Zheng et al. 2002). These consequences of such extraordinary geological and environmental changes for animal and plant life in alpine ecosystems included large geographic range shifts, long periods of isolation, and, in some cases, recent, rapid diversifications (Schoville and Roderick 2009). Because the species abundance of *Parnassius* is much higher than those of other genera in the subfamily Parnassiinae, these "Apollo" butterflies may have experienced a unique evolutionary process in recent geological history (Omoto et al. 2004, Rebourg et al. 2006). Previous studies attempted to associate the *Parnassius* diversification with geological events (such as the rise of the Qinghai-Tibet Plateau and Himalayas, and related orogenies during Cenozoic) and climate changes (such as the Quaternary glaciations) (Condamine et al. 2018b, Favre et al. 2015, Lei et al. 2014, McLean et al. 2018, Omoto et al. 2009). However, it was suggested that current biodiversity has been caused by the joint effect of multiple factors (biogeography, species traits, environmental drivers, and species extinction) rather than a single factor, and that addressing the origin and evolution of the *Parnassius* requires a reliable and accurate phylogenetic framework for pinpointing significant phylogenetic events (Condamine et al. 2018a, 2018b). Although a lot of studies have investigated their phylogeny, the phylogenetic backbone of *Parnassius* has not yet been resolved, and many evolutionary hypotheses were only founded on poorly supported phylogenetic reconstructions (Condamine et al. 2013, 2018b; Nazari et al. 2007; Omoto et al. 2009).

For species identification, the recently developed DNA barcoding technique has been proven useful to corroborate the traditional morphological approaches (Hebert et al. 2003). The method assumes that the genetic variation between two species exceeds that within the species for selected DNA segment (Badotti et al. 2018). *COI* gene is commonly used as the standard barcode for animals and *rbcL*+*matK* for plants; the nuclear internal transcribed spacer (*ITS*) sequences is also recommended as a candidate marker for plant, animal, and fungus species identifications

(Dentinger et al. 2011, Xu 2016, Yao et al. 2010, Zhu et al. 2017). Although the *ITS* in eukaryotes contains two separate regions (*ITS1* and *ITS2*) (Hillis and Dixon 1991), recent studies suggest concerted evolution among them and the *ITS* can be treated as a single gene (Rampersad 2014). Furthermore, it is shown that in both yeasts and fruit flies, *ITS* is essential for the formation of ribosomal subunits and the evolutionary rate is relatively fast (Morgan and Blair 1998, Rampersad 2014). Therefore, *ITS* has been frequently utilized as a marker for phylogenetic analyses at the generic and specific levels (Brown et al. 2000, Coleman 2003, Poczai and Hyvönen 2010).

In the present study, we sequenced *ITS1* and *ITS2* from 267 individuals of 17 *Parnassius* species collected from Qinghai-Tibet Plateau and its neighboring areas. We tested the applicability of *ITS* in species identification of *Parnassius* by analyzing their inter- and intraspecific genetic variation. We used *ITS1* and *ITS2*, for the first time, to reconstruct their phylogeny with multiple methods, and to estimate their divergence times using multiple calibrations with relaxed molecular clock methods, in order to establish a reference framework to evaluate subgenus-level relationships within *Parnassius* and assess the possible geological and palaeoenvironmental events that are likely to be the driving forces for the divergences of *Parnassius* in the region.

Materials and Methods

Sampling and DNA sequencing. We collected 267 adults of 17 *Parnassius* species from various locations in China (Fig. 1; Table 1). Species identification was initially based on morphological traits. Samples used in this study were preserved in the Laboratory of Molecular Evolution and Biodiversity, College of Life Sciences, Anhui Normal University, Wuhu, and Molecular Paleobiology Lab at Nanjing Institute of Geology and Palaeontology, Chinese Academy of Sciences, Nanjing. Genomic DNA was extracted from the leg or thorax tissues using Rapid Animal Genomic DNA Isolation Kit (Sangon Biotech. Co. Ltd, Shanghai, China). The DNA was stored in Tris-EDTA buffer at −20°C.

The amplification of the *ITS1* regions was conducted using polymerase chain reaction (PCR) with the forward primer 18sF1 (5′-TACACACCGCCCGTCGCTACTA-3′) and reverse primer 5.8sB1d (5′-ATGTGCGTTCRAAATGTCGATGTTCA-3′). *ITS2* regions were amplified using the forward primer 5.8sFc (5′-TGAACATCGACATTTYGAACGCACAT-3′) and reverse primer 28sB1d (5′-TTCTTTTCCTCCSCTTAYTRATATGCTTAA-3′) (Ji et al. 2003), in 50 μl reagents containing 6.0 μl 10× PCR buffer, 8.0 μl $MgCl_2$, 1.5 μl dNTPs, 2.0 μl each primer, 1.5 μl DNA template, 1.0 μl Taq DNA polymerase (1.0 U), and 28 μl ddH_2O. The thermal cycle parameters were: an initial denaturation at 95°C for 5 min; followed by 35 cycles: denaturation at 95°C for 50 s, annealing at 59.5°C (*ITS1*) and 54°C (*ITS2*) for 1 min, and extension at 72°C for 2 min; and a final extension at 72°C for 10 min. PCR products were purified using a DNA purification kit (Sangon Biotech. Co. Ltd, Shanghai, China) and sequenced from both directions by General Biosystems Co. Ltd, Anhui, China.

Data analysis. For all *ITS1* and *ITS2* sequences obtained in this study, multiple sequence alignment was conducted by software MAFFT Version 7.1 using the FFT-

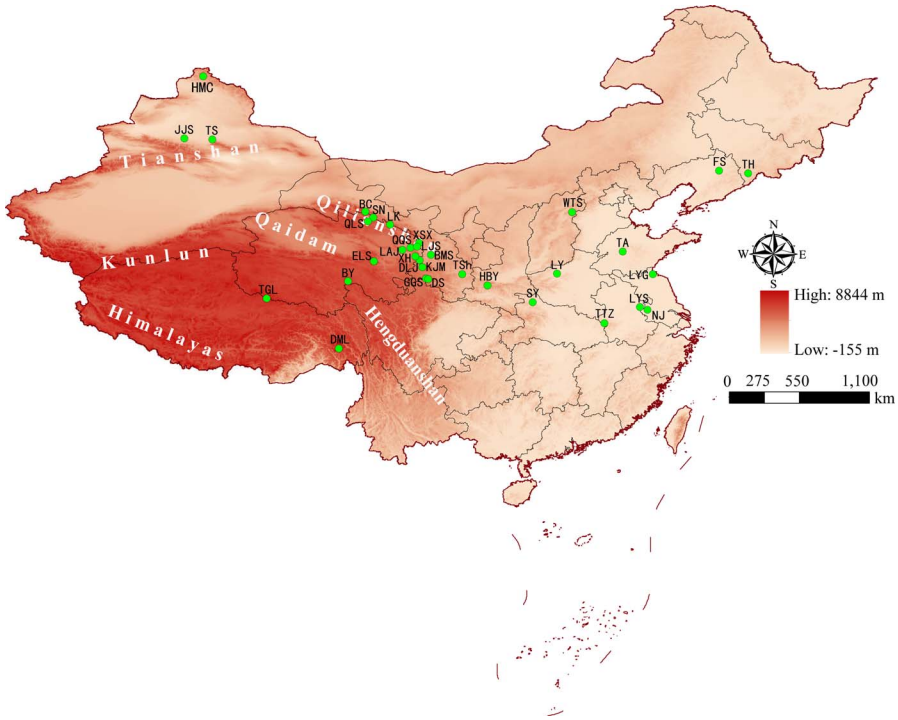

Fig. 1. Sampling localities of the 17 *Parnassius* species used in this study; the code information in the figure refers to Table 1.

NS-i algorithm (Katoh and Standley 2013). The nucleotide composition of the sequences was calculated using MEGA version 7.0 (Kumar et al. 2016). The Kimura 2-parameter (K2P) inter- and intraspecific genetic distances were estimated using MEGA version 7.0. The haplotype diversity (*Hd*), nucleotide diversity (*Pi*), genetic differentiation index (*Fst*), and gene flow (*Nm*) (Grant and Bowen 1998, Slatkin and Maddison 1989, Wright 1965) were analyzed using DnaSP version 6.0 (Rozas et al. 2017). Analysis of molecular variance (AMOVA) was performed by using Arlequin version 3.1 (Excoffier et al. 2005) with 1,000 permutations to compare levels of genetic diversity within and among populations.

Species identification analysis. Six distance parameters were calculated using MEGA version 7.0 for inter- and intraspecific variation, including three parameters for interspecific divergences: (1) average interspecific distance between all species; (2) average theta prime (the mean pairwise distance between all samples); (3) minimum interspecific distance; and three parameters for intraspecific variation: (1) average intraspecific distance among all samples within each species; (2) theta (the mean pairwise distance within each species with at least two representatives); and (3) average coalescent depth (the maximum intraspecific distance within each species with at least two individuals) (Lahaye et al. 2008, Meier et al. 2008, Meyer and Paulay 2005). Distribution of the pairwise inter- and intraspecific distances for *ITS1* and *ITS2* was calculated with the K2P method using the software TaxonDNA

Table 1. List of sample localities of the *Parnassius* species and two other Parnassiinae species used in this study.

Species	Sampling Area	Sampling Time	Code	Longitude (°E)	Latitude (°N)	Sample Size	Haplotypes (Number of Individuals)
Parnassius apollo Linnaeus	Tianshan, Fukang, Xinjiang	2012	TS	E88.074	N44.109	3	AH1(3)
	Hemucun, Buerjin, Xinjiang	2012	HMC	E87.440	N48.574	2	AH2(1) AH3(1)
Parnassius epaphus Oberthür	Bingchuan, Qilian, Qinghai	2016	BC	E98.888	N39.013	6	BH4(6)
	Sunandaban, Yuguzu, Gansu	2016	SN	E99.476	N38.612	5	BH1(4) BH4(1)
	Longkong, Qilian, Qinghai	2016	LK	E100.658	N38.089	8	BH4(6) BH6(2)
	Qilianshan, Tianjun, Qinghai	2014	QLS	E99.094	N38.338	2	BH4(2)
	Bayankalashan, Maduo, Qinghai	2014	BY	E97.662	N34.114	5	BH3(5)
	Guanggaishan, Zhuoni, Gansu	2014	GGS	E103.207	N34.302	5	BH2(3) BH3(1) BH5(1)
	Dalijiashan, Xunhua, Qinghai	2014	DLJ	E102.740	N35.571	6	BH5(6)
Parnassius imperator Oberthür	Qingshashan, Hualong, Qinghai	2014	QSS	E102.087	N36.465	1	CH5(1)

Table 1. Continued.

Species	Sampling Area	Sampling Time	Code	Longitude (°E)	Latitude (°N)	Sample Size	Haplotypes (Number of Individuals)
	Bamishan, Yongjing, Gansu	2014	BMS	E103.517	N35.978	3	CH2(1) CH3(1) CH4(1)
	Kajiaman, Hezuo, Gansu	2014	KJM	E102.911	N35.086	4	CH1(4)
	Guanggaishan, Zhuoni, Gansu	2014	GGS	E103.207	N34.302	1	CH7(1)
	Demulashan, Chayu, Xizang	2017	DML	E97.041	N29.326	1	CH6(1)
Parnassius stubbendorfii Ménétriés	Qingshashan, Hualong, Qinghai	2015	QSS	E102.087	N36.465	5	DH3(5)
	Tonghua, Jilin	2014	TH	E125.947	N41.711	6	DH1(1) DH2(5)
	Fushun, Liaoning	2014	FS	E123.905	N41.894	2	DH4(2)
Parnassius cephalus Grum-Grshimailo	Bingchuan, Qilian, Qinghai	2014	BC	E98.888	N39.013	6	EH3(6)
	Sunandaban, Yuguzu, Gansu	2014	SN	E99.476	N38.612	5	EH1(4) EH2(1)
	Longkong, Qilian, Qinghai	2014	LK	E100.658	N38.089	4	EH4(2) EH5(1) EH6(1)

Table 1. Continued.

Species	Sampling Area	Sampling Time	Code	Longitude (°E)	Latitude (°N)	Sample Size	Haplotypes (Number of Individuals)
	Qilianshan, Tianjun, Qinghai	2014	QLS	E99.094	N38.338	5	EH3(4) EH5(1)
Parnassius nomion Fischer von Waldheim	Bamishan, Yongjing, Gansu	2013	BMS	E103.517	N35.978	5	FH4(5)
	Xiaosanxia, Tianzhu, Gansu	2012	XSX	E102.696	N36.790	1	FH4(1)
	Kajiaman, Hezuo, Gansu	2014	KJM	E102.911	N35.086	5	FH4(5)
	Lijiashan, Haidong, Qinghai	2014	LJS	E102.550	N36.554	1	FH4(1)
	Wutaishan, Wutai, Shanxi	2006	WTS	E113.500	N38.983	4	FH1(1) FH2(1) FH3(2)
Parnassius szechenyii Frivaldszky	Dalijiashan, Xunhua, Qinghai	2015	DLJ	E102.740	N35.571	1	GH1(1)
	Qilianshan, Tianjun, Qinghai	2015	QLS	E99.094	N38.338	1	GH2(1)
Parnassius simo Gray	Bingchuan, Qilian, Qinghai	2016	BC	E98.888	N39.013	2	HH3(2)

Table 1. Continued.

Species	Sampling Area	Sampling Time	Code	Longitude (°E)	Latitude (°N)	Sample Size	Haplotypes (Number of Individuals)
	Sunandaban, Yuguzu, Gansu	2014	SN	E99.476	N38.612	11	HH3(11)
	Longkong, Qilian, Qinghai	2016	LK	E100.658	N38.089	8	HH3(3) HH4(5)
	Elashan, Xinghai, Qinghai	2016	ELS	E99.512	N35.496	6	HH1(2) HH3(2) HH4(2)
	Guanggaishan, Zhuoni, Gansu	2013	GGS	E103.207	N34.302	3	HH2(3)
	Dieshan, Diebu, Gansu	2013	DS	E103.334	N34.269	3	HH2(3)
	Qilianshan, Tianjun, Qinghai	2014	QLS	E99.094	N38.338	6	HH3(3) HH4(3)
Parnassius orleans Oberthür	Bingchuan, Qilian, Qinghai	2016	BC	E98.888	N39.013	5	IH3(1) IH4(4)
	Qingshashan, Hualong, Qinghai	2014	QSS	E102.087	N36.465	3	IH5(1) IH6(2)
	Dalijiashan, Xunhua, Qinghai	2015	DLJ	E102.740	N35.571	4	IH7(1) IH8(1) IH9(1) IH10(1)
	Guanggaishan, Zhuoni, Gansu	2013	GGS	E103.207	N34.302	4	IH10(1) IH11(1) IH12(2)
	Demulashan, Chayu, Xizang	2017	DML	E97.0413	N29.327	4	IH1(3) IH2(1)

Table 1. Continued.

Species	Sampling Area	Sampling Time	Code	Longitude (°E)	Latitude (°N)	Sample Size	Haplotypes (Number of Individuals)
	Lajishan, Guide, Qinghai	2017	LAJ	E101.525	N36.319	2	IH13(1) IH14(1)
Parnassius acdestis Grum-Grshimailo	Guanggaishan, Diebu, Gansu	2013	GGS	E103.207	N34.302	4	JH4(4)
	Dieshan, Diebu, Gansu	2013	DS	E103.334	N34.269	4	JH3(2) JH6(2)
	Bayankalashan, Maduo, Qinghai	2016	BY	E97.662	N34.114	4	JH1(1) JH2(3)
	Xunhua, Haidong, Qinghai	2016	XH	E102.444	N35.836	4	JH5(3) JH6(1)
	Demulashan, Chayu, Xizang	2017	DML	E97.041	N29.326	1	JH7(1)
Parnassius actius Eversmann	Tianshan, Fukang, Xinjiang	2016	TS	E88.074	N44.109	1	KH1(1)
Parnassius choui Huang and Shi	Bayankalashan, Maduo, Qinghai	2015	BY	E97.662	N34.114	2	LH7(2)
	Guanggaishan, Zhuoni, Gansu	2016	GGS	E103.207	N34.302	6	LH8(2) LH9(2) LH10(1) LH11(1)
	Elashan, Xinghai, Qinghai	2015	ELS	E99.512	N35.496	10	LH1(1) LH2(2) LH3(2) LH4(1) LH5(1) LH6(2) LH7(1)

Table 1. Continued.

Species	Sampling Area	Sampling Time	Code	Longitude (°E)	Latitude (°N)	Sample Size	Haplotypes (Number of Individuals)
Parnassius hide Koiwaya	Elashan, Xinghai, Qinghai	2009	ELS	E99.512	N35.496	1	MH1(1)
Parnassius huberi Paulus	Tanggulashan, Anduo, Xizang	2015	TGL	E91.930	N32.877	1	NH1(1)
Parnassius apollonius Eversmann	Jiangjunshan, Shihezi, Xinjiang	2016	JJS	E86.094	N44.203	1	OH1(1)
Parnassius glacialis Butler	Huangbaiyuan, Baoji, Shanxi	2013	HBY	E107.527	N33.815	7	PH1(2) PH26(5)
	Luoyang, Henan	2011	LY	E112.460	N34.631	7	PH11(6) PH26(1)
	Langyashan, Chuzhou, Anhui	2013	LYS	E118.294	N32.286	7	PH2(1) PH3(2) PH4(1) PH5(1) PH6(1) PH7(1)
	Tiantangzhai, Jinzhai, Anhui	2009	TTZ	E115.785	N31.141	7	PH26(2) PH27(2) PH28(2) PH29(1)
	Nanjing, Jiangsu	2016	NJ	E118.845	N32.074	7	PH12(1) PH13(1) PH14(2) PH26(3)
	Lianyungang, Jiangsu	2011	LYG	E119.225	N34.604	7	PH8(1) PH9(1) PH10(1) PH23(2) PH26(2)
	Taian, Shandong	2013	TA	E117.098	N36.208	7	PH18(1) PH19(1) PH20(1) PH21(1) PH22(1) PH23(1) PH24(1)

Table 1. Continued.

Species	Sampling Area	Sampling Time	Code	Longitude (°E)	Latitude (°N)	Sample Size	Haplotypes (Number of Individuals)
	Tianshui, Gansu	2013	TSh	E105.725	N34.589	7	PH24(1) PH25(1) PH26(5)
	Shiyan, Hubei	2016	SY	E110.742	N32.604	7	PH15(2) PH16(1) PH17(2) PH26(2)
Parnassius acco Gray	Qilianshan, Tianjun, Qinghai	2016	QLS	E99.094	N38.338	1	QH1(1)
Sericinus montelus Gray	Tiantangzhai, Jinzhai, Anhui	2011	TTZ	E115.785	N31.141	1	—
Luehdorfia chinensis Leech *	Hangzhou, Zhejiang	—	—	—	—	1	—

* Sequences downloaded from GenBank.

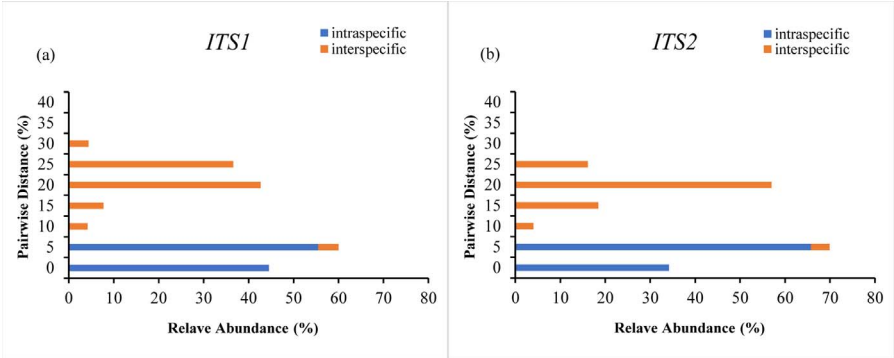

Fig. 2. Relative distribution of the inter- and intraspecific distances for *ITS1* (a) and *ITS2* (b) regions.

version 1.8 (Meier et al. 2006). The barcoding gaps were graphed by the distribution of pairwise inter- and intraspecific distances of the two DNA markers. Species identification ability was evaluated using the "Best match," "Best close match," and "All species barcodes" strategies in TaxonDNA, based on the K2P method (Meier et al. 2006). For the "Best match," a query is assigned the species name of its best-matching barcode sequences, regardless of how similar the query and barcode sequences are; while for the "Best close match," a threshold similarity value is required to define how similar a barcode match needs to be before it can be identified. The "All species barcodes" is the most rigorous application for identifying queries that are assigned a species name only if the query is followed by all known barcodes for a particular species and only if there are at least two conspecific matches (Meier et al. 2006).

Phylogenetic analysis. *Parnassius* phylogeny was reconstructed with the Bayesian inference (BI) and maximum likelihood (ML) methods based on the concatenated *ITS1* and *ITS2* sequence data using *Sericinus montelus* Gray (MN129452 and MN129720) and *Luehdorfia chinensis* Leech (AB071924.1) as the outgroups. Bayesian analysis was performed in MrBayes version 3.2 (Ronquist et al. 2012) under the general time reversible GTR+G nucleotide substitution models determined by PartitionFinder version 1.1.1 (Lanfear et al. 2012). Two independent Markov chain Monte Carlo (MCMC) runs were allowed to go for 4 million generations with sampling each 200th generation. Each run had four chains, one cold and three heated. Convergence of the Bayesian runs was ensured by checking the average standard deviation of split frequencies (StdDev), and the potential scale reduction factor (PSRF) values, and by examining the effective sample size (ESS) of all parameters in Tracer version 1.7.1 (Rambaut et al. 2018). To reach a good convergence, the standard deviation value should be below 0.01, the PSRF value close to 1.00, and the ESS value larger than 200. The first 25% of the sampled generations were discarded as burn-in samples. The resultant posterior probability (BPP) was obtained as the supporting values of each tree node. ML analysis was conducted with software IQ-TREE version 1.6.8 under the GTR+F+R3 models ascertained by the ModelFinder (Kalyaanamoorthy et al. 2017, Nguyen et al. 2014).

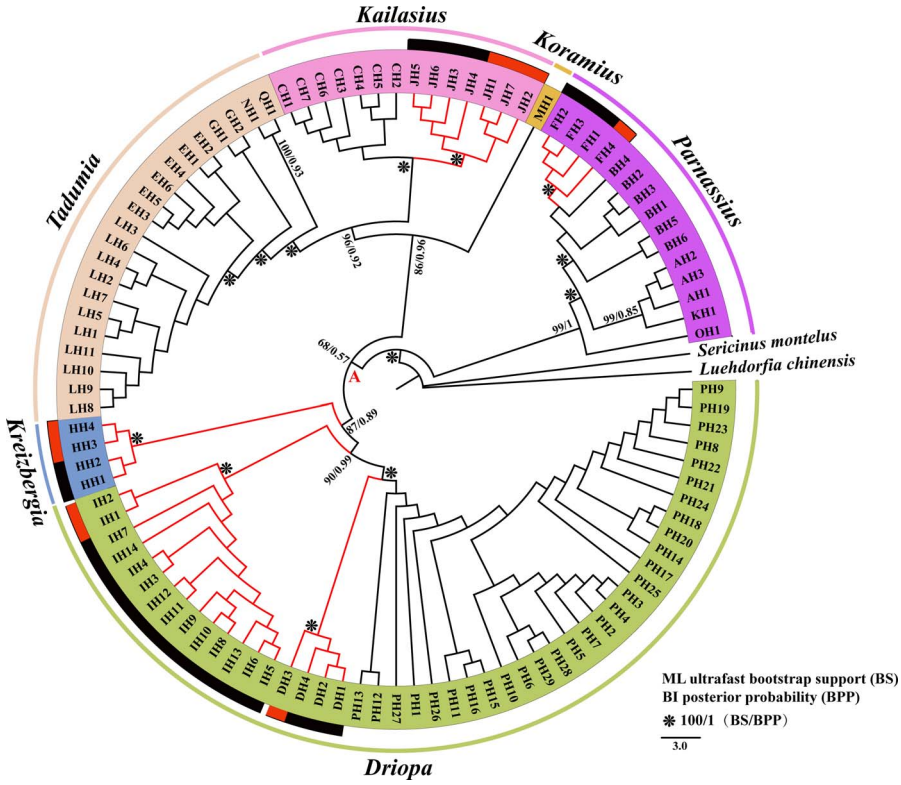

Fig. 3. Bayesian inference (BI) and maximum likelihood (ML) trees inferred from 17 *Parnassius* species based on *ITS1* and *ITS2*. Samples of different colors represent six different subgenera; red and black bars represent different populations within species. Asterisk (*): ML ultrafast bootstrap support values and BI posterior probability values of 100 and 1, respectively.

In the ML analysis, 5,000 ultrafast bootstraps were performed to obtain the ultrafast bootstrap support values (BS) of each node.

Divergence time estimation. The calibrations for the molecular dating were based on two butterfly fossils: *Praepapilio colorado* Durden (Papilionidae) from the Green River Shale of Colorado (USA) of mid-Eocene early Lutetian age (41.2–47.8 Ma) and *Thaites ruminiana* Scudder (subfamily Parnassiinae) from Aix-en-Provence (southern France) of late Oligocene Chattian age (23.03–28.1 Ma) (Condamine et al. 2018b, Durden and Rose 1978, Jong 2017); thus, the crown group divergence of the Parnassiinae was constrained between 23.03 Ma and 47.8 Ma. The earliest divergence time of five *Parnassius* subgenera exclusive of subgenus *Parnassius* was set to be 16–37 Ma according to the divergence time estimates of their host plant *Corydalis* (subfamily Fumarioideae) and the insect–host plant coevolutionary scenario (Pérez-Gutiérrez et al. 2015, Su et al. 2017).

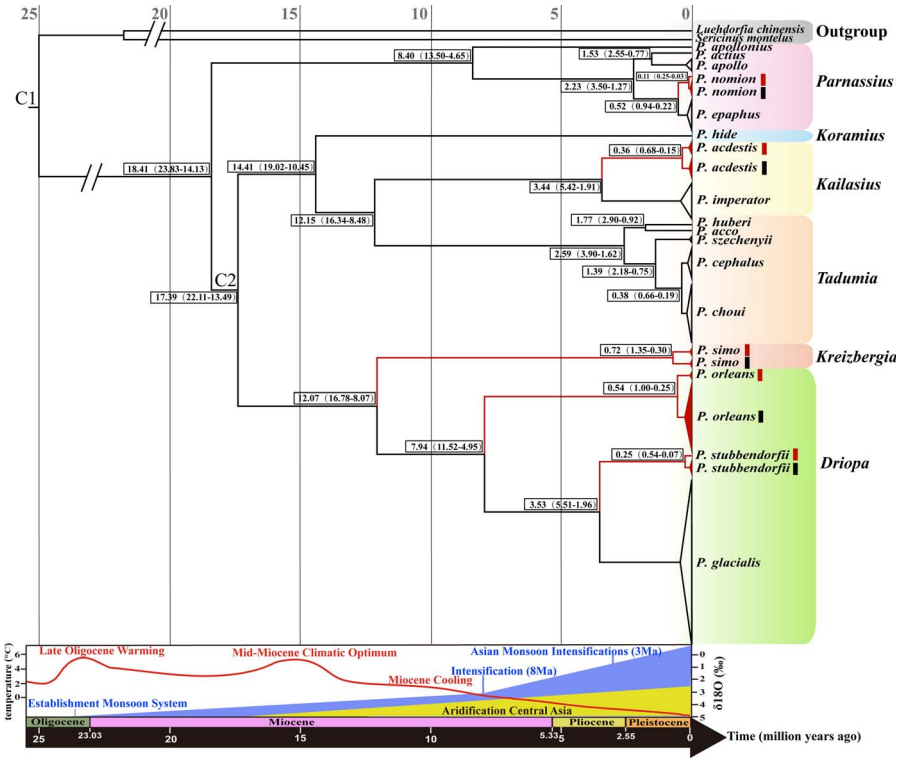

Fig. 4. Phylochronology of *Parnassius* species based on *ITS1* and *ITS2* data under a Bayesian relaxed clock analysis (BEAST, version 1.8.3). C1, C2: calibration points (see text section: Divergence time estimation). Numbers and numbers in parentheses at nodes: median time estimates and 95% confidence interval (CI) in million years ago (Ma), respectively. The red and black bars: different populations within species. Lower graph: The main global temperature curve (Zachos et al. 2001) from the late Oligocene to the Pleistocene with palaeoclimatological information (monsoon and related Central Asian aridification) (from Favre et al. 2015).

Our phylochronological analysis here was conducted using BEAST version 1.8.3 (Drummond et al. 2012) under a relaxed clock model with an uncorrelated lognormal distribution (Drummond et al. 2006). Lognormal priors with soft bounds and 95% confidence intervals (CI) were used for each fossil constraint. The tree prior was set to the birth–death process with incomplete sampling (Stadler 2009), and the nucleotide substitution model was set to the GTR+G model; the MCMC chains were run for 60 million generations with sampling every 1,000 generations; convergence was assessed by Tracer version 1.7.1 (Rambaut et al. 2018), determining whether the ESS of all parameters was larger than 200 as recommended; the nodal heights and maximum credibility tree were generated

with TreeAnnotator version 1.8.3 (Rambaut and Drummond 2016), with the first 6,000 trees being discarded as burn-ins. Finally, the maximum credibility tree was obtained by Figtree version 1.4.3 (Rambaut 2009).

Results

DNA sequence data analysis. The *ITS1* and *ITS2* regions of 267 individuals from 17 *Parnassius* species were successfully sequenced, and annotated and defined by the NCBI database, submitted to and deposited into GenBank (accession No. MN129185–MN129451 and MN129453–MN129719). Our analyses show substantial interspecific variations with the longest (*Parnassius acdestis* Grum-Grshimailo) and shortest (*P. hide* Koiwaya) of *ITS1* sequences being 680 bp and 557 bp, and the longest (*P. acdestis*) and shortest (*P. glacialis* Butler) of *ITS2* sequences being 657 bp and 485 bp in length, respectively (Table 2). On the other hand, intraspecific variations are relatively low, but in a few cases, are significant; for example, the size variation of *P. acdestis ITS1* reached up to 63 bp. Such variations may be attributed to replication slippage, unequal crossing over, and biased gene conversion, as well as geographical isolations and other factors (Hlinka et al. 2002, Platas et al. 2004).

Average AT content of the *ITS2* regions is lower than the *ITS1* regions (52.8% versus 57.7%). For both *ITS1* and *ITS2* sequences, mean AT contents vary remarkably: the highest mean AT content of *ITS1* being 61.5% (*P. glacialis*) and the lowest 54.9% (*P. nomion* Fischer von Waldheim), while the highest and the lowest of *ITS2* are 55.5% (*P. hide*) and 50.2% (*P. imperator* Oberthür), respectively. The total length of the aligned *ITS1* sequences are 792 bp long, with 344 variable sites and 284 parsimony informative sites; while the aligned *ITS2* sequences are 836 bp long, with 315 variable sites and 262 parsimony informative sites.

Species identification. The resulting six distance parameters are shown in Table 3. The results revealed that both *ITS1* and *ITS2* exhibited a relatively higher interspecific and lower intraspecific divergences. For example, the average interspecific and intraspecific distances were 0.2163 and 0.0025 (*ITS1*), and 0.1850 and 0.0024 (*ITS2*), respectively. Although the minimum interspecific distance (0.0023) of the *ITS2* sequences was somewhat less than the maximum intraspecific distance (0.0055), the minimum interspecific distance (0.0062) of the *ITS1* sequences was greater than the maximum intraspecific distance (0.0049). The barcoding gaps between inter- and intraspecific distances are shown in Fig. 2. There was overlap between inter- and intraspecific distances in both *ITS1* and *ITS2* regions. The species identification efficiency of the *ITS1* and *ITS2* regions were tested, as shown in Table 4. The results indicated that under the "Best match" and "Best close match" criteria, the two regions had the same species identification rate of 98.12%; however, both of the region's species identification rates were 97.37% and 83.89%, respectively, using the "All species barcodes" standard.

Genetic differentiation and phylogenetic analysis. The BI and ML trees (Fig. 3) from the *ITS1* + *ITS2* data sets have the same topology, with slight differences of node supporting values, and all the node supporting values were relatively strong (BS $>$ 86%, BPP $>$ 0.85; except node A: BS $=$ 68%, BPP $=$ 0.57). It is shown that the 17 *Parnassius* species are divided into six clades (subgenera) with their

Table 2. Characteristics of the *ITS1* and *ITS2* sequences of 17 *Parnassius* species determined in this study.

		ITS1			*ITS2*		
Species	Number of Individuals	Number of Haplotypes	Length (bp)	Mean AT Content (%)	Number of Haplotypes	Length (bp)	Mean AT Content (%)
Parnassius apollo	5	2	593–596	55.6	2	513	53.4
Parnassius epaphus	37	3	607–608	55.0	4	516	53.8
Parnassius imperator	10	5	660–668	55.5	6	644–650	50.2
Parnassius stubbendorfii	13	3	616–618	59.4	3	487–489	52.9
Parnassius cephalus	20	5	595–617	58.0	3	594–596	51.8
Parnassius nomion	16	3	610	54.9	2	519	53.7
Parnassius szechenyii	2	2	639	57.3	1	602	50.5
Parnassius simo	39	3	576–578	56.5	3	530	50.8
Parnassius orleans	22	7	575–576	57.6	9	510–520	52.6
Parnassius acdestis	17	4	617–680	56.4	5	648–657	51.3
Parnassius actius	1	1	605	55.4	1	521	53.7
Parnassius choui	18	7	613–614	58.0	4	592–594	51.4
Parnassius hide	1	1	557	57.6	1	555	55.5
Parnassius huberi	1	1	595	57.6	1	600	53.2
Parnassius apollonius	1	1	590	56.3	1	496	54.4
Parnassius glacialis	63	13	560–561	61.5	16	485	55.0
Parnassius acco	1	1	610	57.2	1	496	54.0
Total	267	62	557–680	57.7	63	485–657	52.8

Table 3. Inter- and intraspecific variations of *ITS1* and *ITS2* sequences of all individuals of 17 *Parnassius* species.

Parameter	*ITS1*	*ITS2*
Average interspecific distance	0.2163 ± 0.0809	0.1850 ± 0.0675
Theta prime	0.1849 ± 0.0910	0.1634 ± 0.0793
Minimum interspecific distance	0.0062	0.0023
Average intraspecific distance	0.0025 ± 0.0015	0.0024 ± 0.0018
Theta	0.0026 ± 0.0015	0.0024 ± 0.0018
Coalescent depth	0.0049	0.0055

relationship as follows: (([*Driopa* + *Kreizbergia*] + [*Kailasius* + *Tadumia*] + *Koramius*)) + *Parnassius*). The five *Parnassius* species (*P. stubbendorfii* Ménétriés, *P. nomion*, *P. simo* Gray, *P. orleans* Oberthür, *P. acdestis*) with different populations all contain two major geographic branches (Fig. 3, red branches).

The interspecific genetic distances among 17 *Parnassius* species and the genetic distance within and among populations of the five *Parnassius* species are shown in Tables 5 and 6, respectively. The results revealed that the interspecific

Table 4. Species identification efficiency of *ITS1* and *ITS2* regions in *Parnassius*.

Item	*ITS1*	*ITS2*
Individuals	267	267
Best match		
Correct (%)	98.12	98.12
Ambiguous (%)	0	0
Incorrect (%)	1.87	1.87
Best close match		
Correct (%)	98.12	98.12
Ambiguous (%)	0	0
Incorrect (%)	0.37	0
All species barcodes		
Correct (%)	97.37	83.89
Ambiguous (%)	0.74	14.23
Incorrect (%)	0.37	0

Table 5. Kimura 2-Parameter genetic distance among 17 *Parnassius* species in this study.

	1	2	3	4	5	6	7	8	9	10	11	12	13	14	15	16	17
1 *P. apollo*																	
2 *P. epaphus*	0.032																
3 *P. imperator*	0.221	0.232															
4 *P. stubbendorfii*	0.195	0.212	0.250														
5 *P. cephalus*	0.248	0.255	0.260	0.228													
6 *P. nomion*	0.036	0.008	0.237	0.212	0.261												
7 *P. szechenyii*	0.238	0.248	0.265	0.221	0.027	0.254											
8 *P. simo*	0.183	0.188	0.204	0.175	0.224	0.190	0.221										
9 *P. orleans*	0.165	0.176	0.201	0.102	0.189	0.176	0.183	0.133									
10 *P. acdestis*	0.212	0.221	0.063	0.237	0.258	0.227	0.263	0.193	0.191								
11 *P. actius*	0.029	0.039	0.243	0.198	0.268	0.041	0.261	0.192	0.177	0.240							
12 *P. choui*	0.248	0.255	0.259	0.227	0.006	0.261	0.029	0.218	0.188	0.259	0.265						
13 *P. hide*	0.267	0.275	0.219	0.249	0.258	0.277	0.257	0.232	0.205	0.212	0.289	0.256					
14 *P. huberi*	0.256	0.261	0.267	0.244	0.044	0.266	0.041	0.227	0.200	0.255	0.277	0.045	0.269				
15 *P. apollonius*	0.129	0.136	0.244	0.215	0.260	0.140	0.240	0.207	0.182	0.231	0.140	0.260	0.248	0.246			
16 *P. glacialis*	0.212	0.228	0.252	0.072	0.238	0.228	0.236	0.177	0.125	0.240	0.219	0.239	0.240	0.264	0.237		
17 *P. acco*	0.287	0.294	0.270	0.266	0.050	0.299	0.044	0.243	0.208	0.258	0.310	0.052	0.279	0.038	0.287	0.273	

Table 6. Analysis of intraspecific genetic differentiation* of the five *Parnassius* species.

Species	*Dh* Mean (Range)	*Dp* Mean (Range)	*Hd*	*Pi*	*Fst*	*Nm*
Parnassius stubbendorfii	0	0.0036 (0.0009–0.0055)	0.667	0.00258	1.0000	0
Parnassius nomion	0.0003 (0–0.0009)	0.0005 (0–0.0013)	0.442	0.00058	0.6667	0.13
Parnassius simo	0.0012 (0–0.0074)	0.0075 (0–0.0148)	0.634	0.00494	0.8395	0.05
Parnassius orleans	0.0007 (0–0.0018)	0.0040 (0.0012–0.0080)	0.909	0.00364	0.8203	0.05
Parnassius acdestis	0.0004 (0–0.0012)	0.0031 (0.0004–0.0051)	0.816	0.00245	0.8506	0.04

* *Dh*, genetic distance within geographic populations; *Dp*, genetic distance among different geographic populations; *Hd*, haplotype diversity; *Pi*, nucleotide diversity; *Fst*, genetic differentiation index; *Nm*, gene flow.

Table 7. Analysis of molecular variance of genetic variance among different populations of the five *Parnassius* species.

Species	Source of Variation	Sum of Squares	Variance Components	Percentage of Variation	*P*-Value
Parnassius stubbendorfii	Among populations	23.410	2.88462	94.54	0
	Within populations	1.667	0.16667	5.46	
Parnassius nomion	Among populations	3.375	0.24081	63.85	0.003
	Within populations	1.500	0.13636	36.15	
Parnassius simo	Among populations	90.471	2.68756	76.76	0
	Within populations	26.042	0.81380	23.24	
Parnassius orleans	Among populations	77.665	4.03365	81.12	0
	Within populations	15.017	0.93854	18.88	
Parnassius acdestis	Among populations	181.662	12.22470	70.38	0
	Within populations	61.750	5.14583	29.62	

genetic distances ranged from 0.006 (between *P. cephalus* Grum-Grshimailo and *P. choui* Huang and Shi) to 0.310 (between *P. actius* Eversmann and *P. acco* Gray), and the genetic distance within populations of the five *Parnassius* species were significantly smaller than those among populations. The haplotype diversity (*Hd*) of the total population of the five *Parnassius* species ranged from 0.442 to 0.909, and the nucleotide diversity (*Pi*) ranged from 0.00058 to 0.00494 (Table 6). AMOVA showed that the genetic variation among populations of the five *Parnassius* species was significantly greater than those within population ($P \leq 0.003$) (Table 7). The total population genetic differentiation index (*Fst*) and gene flow (*Nm*) of the five *Parnassius* species ranged from 0.6667 to 1.0000 and 0 to 0.13 (Table 6), respectively.

Divergence time analysis. As shown in our relaxed molecular clock analysis using C1 (divergence of the subfamily Parnassiinae) and C2 (divergence of the genus *Parnassius* exclusive of subgenus *Parnassius*) as the calibration points (Fig. 4), the diversification time of genus *Parnassius* (i.e., the splitting of subgenus *Parnassius* and other subgenera) started about 18.41 Ma (95% CI: 23.83–14.13 Ma) in early Miocene. The divergence of two major clades (subgenera *Driopa* + *Kreizbergia* versus *Tadumia* + *Kailasius* + *Koramius*) within genus *Parnassius* occurred about 17.39 Ma (95% CI: 22.11–13.49 Ma) during early Miocene to mid-Miocene, followed by the splitting of subgenus *Koramius* from the clade of *Kailasius* + *Tadumia* about 14.41 Ma (95% CI: 19.02–10.45 Ma), and *Kailasius* from *Tadumia*

about 12.15 Ma (95% CI: 16.34–8.48 Ma). Subgenus *Kreizbergia* diverged from *Driopa* about 12.07 Ma (95% CI: 16.78–8.07 Ma). According to our divergence data analysis, the interspecific divergences of the 17 *Parnassius* species and intraspecific differentiations of the five *Parnassius* species mostly concentrated from about 3.5 Ma and earlier during late Pliocene and Quaternary time, when the global temperature continually declined (Fig. 4, lower graph) associated with widespread glaciation.

Discussion

Species identification. Previous studies have shown that ideal candidate DNA barcodes should, first, have sufficient variations to discriminate among species and also need to be sufficiently conserved so that there is less variability within species than between species. Second, ideal DNA barcodes should harbor a "barcode gap," where the distribution of intraspecific variation and interspecific divergence have discrete distributions and no overlap. Third, they should have a high success rate of species identification (Hartvig et al. 2015, Hebert et al. 2003, Meier et al. 2008, Meyer and Paulay 2005, Yao et al. 2010). In the present study, our *ITS1* and *ITS2* regions presented the most promising universal DNA barcodes for authenticating *Parnassius* species as assessed by several criteria. First, determination of genetic divergence using six distance parameters confirmed that the *ITS1* and *ITS2* regions possessed high interspecific divergences and low intraspecific variations (Table 3). Second, DNA barcoding gaps analyses indicated that there existed slight overlaps between inter- and intraspecific distances for the two evaluated regions (Fig. 2). Third, species identification efficiency via three common criteria ("Best match," "Best close match," and "All species barcodes") as suggested by Meier et al. (2006) indicated that both *ITS1* and *ITS2* harbored significantly high species identification rates (98.12%) and were able to correctly identify 261 out of 267 individuals using the "Best match" and "Best close match" criteria; however, under the "All species barcodes" standard, the correct identification rate of *ITS2* region (83.89%) was slightly low and *ITS1* higher (97.37%) (Table 4). Overall, our newly determined *ITS1* and *ITS2* markers are useful and reasonably efficient to *Parnassius* species identification.

Genetic differentiation and phylogenetic analysis. In this study, the basal position of subgenus *Parnassius* is congruent with results obtained by Omoto et al. (2004), Rebourg et al. (2006), Michel et al. (2008), and Condamine et al. (2018b). However, the relationships among other subgenera resolved in this study differ from previous studies, prompting further studies with more comprehensive data sets to resolve.

The species relationships within each subgenus obtained in this study based on *ITS* data essentially conform to the traditional morphological classifications, as also shown in Omoto et al. (2004), Katoh et al. (2005), Michel et al. (2008), and Zheng et al. (2018), based on mitochondrial or mitochondrial plus nuclear gene sequence data. Our analyses also suggest that *P. acdestis* belongs to subgenus *Kailasius* instead of subgenus *Koramius*, despite the similar morphology in wing venation and sphragis, verifying the analysis by Omoto et al. (2009) based on mitochondrial data.

The haplotype diversity (*Hd*) and the nucleotide diversity (*Pi*) analysis of the total population of the five *Parnassius* species showed that they all harbored a relatively low level of nucleotide diversity ($Pi < 0.005$) and a high level of haplotype diversity ($Hd > 0.5$) except for *P. nomion* (Table 6). AMOVA indicated that their genetic variations came mainly from different geographical populations (Table 7), and the results correspond to the those of the genetic distance. The total population genetic differentiation index (*Fst*) and gene flow (*Nm*) analysis suggested that their genetic differentiation levels were significantly high ($Fst > 0.25$) with relatively limited gene flows ($Nm < 1$) (Table 6).

Divergence time analysis. Our phylochronological results (Fig. 4) generally agree with those of Condamine et al. (2013), who determined the earliest *Parnassius* divergence at about 17 Ma (95% CI: 22–13 Ma), but significantly differed from the results obtained by Nazari et al. (2007), Omoto et al. (2009), and Condamine et al. (2018b), who provided dates of the same event at about 39–34 Ma (late Eocene), 24.3 Ma (late Oligocene), and 13.4 Ma (95% CI: 16.6–10.5 Ma) (middle Miocene), respectively. We found that the major source of differences in dating the tree came from calibration points and their distribution in the tree. In this analysis, we adopted, in our calibration system (Fig. 4), high-quality fossil dates of Papilionidae and Parnassiinae and relevant dates from the host plants (*Corydalis*) based on the coevolution perspective, which are likely better proxies approaching the true reference time frame.

The uplift of the Qinghai-Tibetan Plateau and Himalayas caused a dramatic climatic and ecological shift. The forests were replaced by grasslands, and the climate gradually became drier, colder, and windier; glaciers started to develop, deserts formed (Wu et al. 2001); and accordingly, an area of worldwide importance for biodiversity in the Qinghai-Tibetan Plateau gradually developed, due to the unique geomorphologic configuration, complex land and climate conditions, as well as the distinct geological history that gave rise to the endemic, specialized montane animal and plant species (Lei et al. 2014).

In this study, the estimated divergences of *Parnassius* coincide and are likely related with geological events in the distribution regions of the butterflies, especially the progressive uplifting of the Himalayas and the Qinghai-Tibet Plateau during the early to middle Miocene (20–10 Ma) (Favre et al. 2015, Lu and Guo 2014, Molnar and Stock 2009). Studies show that these geological events remarkably changed the atmospheric circulations that gave rise to the intensified Asian monsoon and Central Asian aridification (Guo et al. 2008, Miao et al. 2012, Sun and Wang 2005, Wan et al. 2007). Afterwards, the two profound strengthening of these two events were accompanied by large-scale cooling of the Asian continent, which occurred at about 8 Ma and 3 Ma in the late Miocene and late Pliocene, respectively; and the latter event (3 Ma) may have been related to the *Parnassius* interspecific divergences for the extant species in our samples (Guo et al. 2011, Herbert et al. 2016, Wan et al. 2007). Meanwhile, the Tibet Movement between 3.6 and 1.7 Ma may also be responsible for interspecific genetic differentiation and speciation in the genus (Li et al. 1996).

The climatic oscillations in the Quaternary had profound effects on the organisms now inhabiting alpine ecosystems (Hewitt 2000). Numerous studies have documented effects of climatic cycles on population genetic diversifications, as well as both recent and ancient speciation events in alpine organisms (Chiocchio

et al. 2017, DeChaine and Martin 2006, Sandel et al. 2011, Schoville and Roderick 2009). For example, the systematics and biogeography studies of *Parnassius phoebus* complexes in North America showed that *P. smintheus* Doubleday and *P. behrii* Edwards differentiated in the Pleistocene due to alpine glaciers (Schoville and Roderick 2009). The Qinghai-Tibetan Plateau region was more strongly affected by the widespread Quaternary glaciations than other regions of the world (Lei et al. 2014, Owen and Dortch 2014, Yang et al. 2008, Zhou et al. 2006), and the related geological events such as the Kunlun-Yellow River Tectonic Movement (1.1–0.6 Ma) (Wu et al. 2001, Zhou et al. 2006) are likely responsible for the habitat fragmentation and isolation of the *Parnassius* species and intraspecific differentiations of this study, judging from their space and time agreement between the butterfly phylogenesis and the paleoenvironmental events in the region.

Acknowledgments

This work was supported by the National Natural Science Foundation of China (41972029, 41472028), and the funds from the Strategic Priority Research Program of the Chinese Academy of Sciences (XDB26000000).

References Cited

Badotti, F., P.L.C. Fonseca, L.M.R. Tomé, D.T. Nunes and A. Góes-Neto. 2018. ITS and secondary biomarkers in fungi: Review on the evolution of their use based on scientific publications. Braz. J. Bot. 41: 471–479.

Brown, B., R. Emberson and A. Paterson. 2000. Phylogenetic relationships within the genus *Wiseana* (Lepidoptera: Hepialidae). N. Z. J. Zool. 27: 1–14.

Chiocchio, A., R. Bisconti, M. Zampiglia, G. Nascetti and D. Canestrelli. 2017. Quaternary history, population genetic structure and diversity of the cold-adapted Alpine newt *Ichthyosaura alpestris* in peninsular Italy. Sci. Rep. 7: 2955.

Chou, I. 1999. Monographia Rhopalocerorum Sinensium. Henan Scientific and Technological Publishing House, Zhenzhou, China. 191 pp.

Coleman, A.W. 2003. ITS2 is a double-edged tool for eukaryote evolutionary comparisons. Trends Genet. 19: 370–375.

Condamine, F.L. 2018. Limited by the roof of the world: Mountain radiations of Apollo swallowtails controlled by diversity-dependence processes. Biol. Lett. 14: 20170622.

Condamine, F.L., B. Nabholz, A.L. Clamens, J.R. Dupuis and F.A.H. Sperling. 2018a. Mitochondrial phylogenomics, the origin of swallowtail butterflies, and the impact of the number of clocks in Bayesian molecular dating. Syst. Entomol. 43: 460–480.

Condamine, F.L., J. Rolland, S. Höhna, F.A.H. Sperling and I. Sanmartín. 2018b. Testing the role of the Red Queen and Court Jester as drivers of the macroevolution of Apollo butterflies. Syst. Biol. 67: 940–964.

Condamine, F.L., F.A.H. Sperling and G.J. Kergoat. 2013. Global biogeographical pattern of swallowtail diversification demonstrates alternative colonization routes in the Northern and Southern hemispheres. J. Biogeogr. 40: 9–23.

DeChaine, E.G. and A.P. Martin. 2006. Using coalescent simulations to test the impact of Quaternary climate cycles on divergence in an alpine plant–insect association. Evolution 60: 1004–1013.

Dentinger, B.T.M., M.Y. Didukh and J.M. Moncalvo. 2011. Comparing COI and ITS as DNA barcode markers for mushrooms and allies (*Agaricomycotina*). PLoS ONE 6: e25081.

Drummond, A.J., S.Y.W. Ho, M.J. Phillips and A. Rambaut. 2006. Relaxed phylogenetics and dating with confidence. PLoS Biol. 4: e88.

Drummond, A.J., M.A. Suchard, D. Xie and A. Rambaut. 2012. Bayesian phylogenetics with BEAUti and the BEAST 1.7. Mol. Biol. Evol. 29: 1969–1973.

Du, K., L.R. Yang, R. Zhang, L.P. Yue, H.J. Guo, Y.X. Zhang, J.X. Li and H.J. Gong. 2019. Cenozoic tectonics and landform evolution in the Qilian Mountains and adjacent areas. Int. Geol. Rev. doi: 10.1080/00206814.2019.1627588.

Durden, C.J. and H. Rose. 1978. Butterflies from the middle Eocene: The earliest occurrence of fossil Papilionoidea (Lepidoptera). Pearce-Sellards Ser. Tex. Mem. Mus. 29: 1–25.

Excoffier, L., G. Laval and S. Schneider. 2005. Arlequin (version 3.0): An integrated software package for population genetics data analysis. Evol. Bioinform. Online 1: 47–50.

Favre, A., M. Päckert, S.U. Pauls, S.C. Jähnig, D. Uhl, I. Michalak and A.N. Muellner-Riehl. 2015. The role of the uplift of the Qinghai-Tibetan Plateau for the evolution of Tibetan biotas. Biol. Rev. 90: 236–253.

Grant, W.S. and B.W. Bowen. 1998. Shallow population histories in deep evolutionary lineages of marine fishes: Insights from sardines and anchovies and lessons for conservation. J. Hered. 89: 415–426.

Guo, X.G., X. Dai, D. Chen, T.J. Papenfuss, N.B. Ananjeva, D.A. Melnikov and Y.Z. Wang. 2011. Phylogeny and divergence times of some racerunner lizards (Lacertidae: *Eremias*) inferred from mitochondrial 16S rRNA gene segments. Mol. Phylogenet. Evol. 61: 400–412.

Guo, Z.T., B. Sun, Z.S. Zhang, S.Z. Peng, G.Q. Xiao, J.Y. Ge, Q.Z. Hao, Y.S. Qiao, M.Y. Liang and J.F. Liu. 2008. A major reorganization of Asian climate by the early Miocene. Clim. Past 4: 153–174.

Hartvig, I., M. Czako, E.D. Kjær, L.R. Nielsen and I. Theilade. 2015. The use of DNA barcoding in identification and conservation of rosewood (*Dalbergia spp.*). PLoS ONE 10: e0138231.

Hebert, P.D.N., A. Cywinska, S.L. Ball and J.R. Dewaard. 2003. Biological identifications through DNA barcodes. Proc. R. Soc. Lond. B Biol. Sci. 270: 313–321.

Herbert, T.D., K.T. Lawrence, A. Tzanova, L.C. Peterson, R. Caballero-Gill and C.S. Kelly. 2016. Late Miocene global cooling and the rise of modern ecosystems. Nat. Geosci. 9: 843–847.

Hewitt, G. 2000. The genetic legacy of the Quaternary ice ages. Nature 405: 907–913.

Hillis, D.M. and M.T. Dixon. 1991. Ribosomal DNA: Molecular evolution and phylogenetic inference. Q. Rev. Biol. 66: 411–453.

Hlinka, O., A. Murrell and S.C. Barker. 2002. Evolution of the secondary structure of the rRNA internal transcribed spacer 2 (ITS2) in hard ticks (Ixodidae, Arthropoda). Heredity 88: 275–279.

Ji, Y.J., D.X. Zhang and L.J. He. 2003. Evolutionary conservation and versatility of a new set of primers for amplifying the ribosomal internal transcribed spacer regions in insects and other invertebrates. Mol. Ecol. Notes 3: 581–585.

Jong, R.D. 2017. Fossil butterflies, calibration points and the molecular clock (Lepidoptera: Papilionoidea). Zootaxa 4270: 1–63.

Kalyaanamoorthy, S., B.Q. Minh, T.K.F. Wong, A.V. Haeseler and L.S. Jermiin. 2017. ModelFinder: Fast model selection for accurate phylogenetic estimates. Nat. Methods 14: 587–589.

Katoh, K. and D.M. Standley. 2013. MAFFT multiple sequence alignment software version 7: Improvements in performance and usability. Mol. Biol. Evol. 30: 772–780.

Katoh, T., A. Chichvarkhin, T. Yagi and K. Omoto. 2005. Phylogeny and evolution of butterflies of the genus *Parnassius* inferences from mitochondrial 16S and ND1 sequences. Zool. Sci. 22: 343–351.

Kumar, S., G. Stecher and K. Tamura. 2016. MEGA7: Molecular evolutionary genetics analysis version 7.0 for bigger datasets. Mol. Biol. Evol. 33: 1870–1874.

Lahaye, R., M.V.D. Bank, D. Bogarin, J. Warner, F. Pupulin, G. Gigot, O. Maurin, S. Duthoit, T.G. Barraclough and V. Savolainen. 2008. DNA barcoding the floras of biodiversity hotspots. Proc. Natl. Acad. Sci. USA 105: 2923–2928.

Lanfear, R., B. Calcott, S.Y. Ho and S. Guindon. 2012. PartitionFinder: Combined selection of partitioning schemes and substitution models for phylogenetic analyses. Mol. Biol. Evol. 29: 1695–1701.

Lei, F.M., Y.H. Qu and G. Song. 2014. Species diversification and phylogeographical patterns of birds in response to the uplift of the Qinghai-Tibet Plateau and Quaternary glaciations. Curr. Zool. 60: 149–161.

Li, J.J., X.M. Fang, H.Z. Ma, J.J. Zhu, B.T. Pan and H.L. Chen. 1996. Geomorphological and environmental evolution in the upper reaches of the Yellow River during the late Cenozoic. Sci. China Ser. D 39: 380–390.

Lu, H.Y. and Z.T. Guo. 2014. Evolution of the monsoon and dry climate in East Asia during late Cenozoic: A review. Sci. China Earth Sci. 57: 70–79.

McLean, B.S., B. Nyamsuren, A. Tchabovsky and J.A. Cook. 2018. Impacts of late Quaternary environmental change on the long-tailed ground squirrel (*Urocitellus undulatus*) in Mongolia. Zool. Res. 39: 364–372.

Meier, R., K. Shiyang, G. Vaidya and P.K.L. Ng. 2006. DNA barcoding and taxonomy in Diptera: A tale of high intraspecific variability and low identification success. Syst. Biol. 55: 715–728.

Meier, R., G.Y. Zhang and F. Ali. 2008. The use of mean instead of smallest interspecific distances exaggerates the size of the "barcoding gap" and leads to misidentification. Syst. Biol. 57: 809–813.

Meyer, C.P. and G. Paulay. 2005. DNA barcoding: Error rates based on comprehensive sampling. PLoS Biol. 3: e422.

Miao, Y.F., M. Herrmann, F.L. Wu, X.L. Yan and S.L. Yang. 2012. What controlled Mid-Late Miocene long-term aridification in Central Asia?—Global cooling or Tibetan Plateau uplift: A review. Earth-Sci. Rev. 112: 155–172.

Michel, F., C. Rebourg, E. Cosson and H. Descimon. 2008. Molecular phylogeny of Parnassiinae butterflies (Lepidoptera: Papilionidae) based on the sequences of four mitochondrial DNA segments. Ann. Soc. Entomol. Fr. 44: 1–36.

Molnar, P. and J.M. Stock. 2009. Slowing of India's convergence with Eurasia since 20 Ma and its implications for Tibetan mantle dynamics. Tectonics 28: TC3001.

Morgan, J.A.T. and D. Blair. 1998. Trematode and monogenean rRNA ITS2 secondary structures support a four-domain model. J. Mol. Evol. 47: 406–419.

Najman, Y., E. Appel, M. Boudagher-Fadel, P. Bown, A. Carter, E. Garzanti, L. Godin, J.T. Han, U. Liebke and G. Oliver. 2010. Timing of India-Asia collision: Geological, biostratigraphic, and palaeomagnetic constraints. J. Geophys. Res. 115: B12416.

Nazari, V., E.V. Zakharov and F.A.H. Sperling. 2007. Phylogeny, historical biogeography, and taxonomic ranking of Parnassiinae (Lepidoptera, Papilionidae) based on morphology and seven genes. Mol. Phylogenet. Evol. 42: 131–156.

Nguyen, L.T., H.A. Schmidt, A.V. Haeseler and B.Q. Minh. 2014. IQ-TREE: A fast and effective stochastic algorithm for estimating maximum-likelihood phylogenies. Mol. Biol. Evol. 32: 268–274.

Omoto, K., T. Katoh, A. Chichvarkhin and T. Yagi. 2004. Molecular systematics and evolution of the "Apollo" butterflies of the genus *Parnassius* (Lepidoptera: Papilionidae) based on mitochondrial DNA sequence data. Gene 326: 141–147.

Omoto, K., T. Yonezawa and T. Shinkawa. 2009. Molecular systematics and evolution of the recently discovered "Parnassian" butterfly (*Parnassius davydovi* Churkin, 2006) and its allied species (Lepidoptera, Papilionidae). Gene 441: 80–88.

Owen, L.A. and J.M. Dortch. 2014. Nature and timing of Quaternary glaciation in the Himalayan-Tibetan orogen. Quat. Sci. Rev. 88: 14–54.

Pérez-Gutiérrez, M.A., A.T. Romero-García, M.C. Fernández, G. Blanca, M.J. Salinas-Bonillo and V.N. Suárez-Santiago. 2015. Evolutionary history of fumitories (subfamily Fumarioideae, Papaveraceae): An old story shaped by the main geological and climatic events in the Northern Hemisphere. Mol. Phylogenet. Evol. 88: 75–92.

Platas, G., C. Ruibal and J. Collado. 2004. Size and sequence heterogeneity in the ITS1 of *Xylaria hypoxylon* isolates. Mycol. Res. 108: 71–75.

Poczai, P. and J. Hyvönen. 2010. Nuclear ribosomal spacer regions in plant phylogenetics: Problems and prospects. Mol. Biol. Rep. 37: 1897–1912.

Rambaut, A. 2009. FigTree version 1.4: Tree figure drawing tool. Institute Evol. Biol., Univ. Edinburgh, Edinburgh, Scotland. http://tree.bio.ed.ac.uk/ (accessed 01 November 2019).

Rambaut, A. and A. Drummond. 2016. TreeAnnotator version 1.8.3. http://beast.bio.ed.ac.uk/TreeAnnotator (accessed 01 November 2019).

Rambaut, A., A.J. Drummond, D. Xie, G. Baele and M.A. Suchard. 2018. Posterior summarization in Bayesian phylogenetics using Tracer 1.7. Syst. Biol. 67: 901–904.

Rampersad, S.N. 2014. ITS1, 5.8 S and ITS2 secondary structure modelling for intra-specific differentiation among species of the *Colletotrichum gloeosporioides sensu lato* species complex. SpringerPlus 3: 684.

Rebourg, C., F. Péténian, E. Cosson and E. Faure. 2006. Patterns of speciation and adaptive radiation in *Parnassius* butterflies. J. Entomol. 3: 204–215.

Ronquist, F., M. Teslenko, P.V.D. Mark, D.L. Ayres, A. Darling, S. Höhna, B. Larget, L. Liu, M.A. Suchard and J.P. Huelsenbeck. 2012. MrBayes 3.2: Efficient Bayesian phylogenetic inference and model choice across a large model space. Syst. Biol. 61: 539–542.

Rozas, J., A. Ferrer-Mata, J.C. Sánchez-DelBarrio, S. Guirao-Rico, P. Librado, S.E. Ramos-Onsins and A. Sánchez-Gracia. 2017. DnaSP 6: DNA sequence polymorphism analysis of large data sets. Mol. Biol. Evol. 34: 3299–3302.

Sandel, B., L. Arge, B. Dalsgaard, R.G. Davies, K.J. Gaston, W.J. Sutherland and J.C. Svenning. 2011. The influence of Late Quaternary climate-change velocity on species endemism. Science 334: 660–664.

Schoville, S.D. and G.K. Roderick. 2009. Alpine biogeography of Parnassian butterflies during Quaternary climate cycles in North America. Mol. Ecol. 18: 3471–3485.

Shi, Y.F. 2002. Characteristics of late Quaternary monsoonal glaciation on the Tibetan Plateau and in East Asia. Quat. Int. 97–98: 79–91.

Slatkin, M. and W.P. Maddison. 1989. A cladistic measure of gene flow inferred from the phylogenies of alleles. Genetics 123: 603–613.

Stadler, T. 2009. On incomplete sampling under birth-death models and connections to the sampling-based coalescent. J. Theor. Biol. 261: 58–66.

Su, C.Y., Q.H. Shi, X.Y. Sun, J.Y. Ma, C.X. Li, J.S. Hao and Q. Yang. 2017. Dated phylogeny and dispersal history of the butterfly subfamily Nymphalinae (Lepidoptera: Nymphalidae). Sci. Rep. 7: 8799.

Sun, X.J. and P.X. Wang. 2005. How old is the Asian monsoon system?—Palaeobotanical records from China. Palaeogeogr., Palaeoclimatol., Palaeoecol. 222: 181–222.

Wan, S.M., A.C. Li, P.D. Clift and J.B.W. Stuut. 2007. Development of the East Asian monsoon: Mineralogical and sedimentologic records in the northern South China Sea since 20 Ma. Palaeogeogr., Palaeoclimatol., Palaeoecol. 254: 561–582.

Wright, S. 1965. The interpretation of population structure by F-statistics with special regard to systems of mating. Evolution 19: 395–420.

Wu, Y.Q., Z.J. Cui, G.N. Liu, D.K. Ge, J.R. Yin, Q.H. Xu and Q.Q. Pang. 2001. Quaternary geomorphological evolution of the Kunlun Pass area and uplift of the Qinghai-Xizang (Tibet) Plateau. Geomorphology 36: 203–216.

Xu, J.P. 2016. Fungal DNA barcoding. Genome 59: 913–932.

Xu, L.B., X.J. Ou, Z.P. Lai, S.Z. Zhou, J. Wang and Y. Fu. 2010. Timing and style of Late Pleistocene glaciation in the Queer Shan, northern Hengduan Mountains in the eastern Tibetan Plateau. J. Quat. Sci. 25: 957–966.

Yang, F.S., Y.F. Li, X. Ding and X.Q. Wang. 2008. Extensive population expansion of *Pedicularis longiflora* (Orobanchaceae) on the Qinghai-Tibetan Plateau and its correlation with the Quaternary climate change. Mol. Ecol. 17: 5135–5145.

Yao, H., J.Y. Song, C. Liu, K. Luo, J.P. Han, Y. Li, X.H. Pang, H.X. Xu, Y.J. Zhu and P.G. Xiao. 2010. Use of ITS2 region as the universal DNA barcode for plants and animals. PLoS ONE 5: e13102.

Zachos, J., M. Pagani, L. Sloan, E. Thomas and K. Billups. 2001. Trends, rhythms, and aberrations in global climate 65 Ma to present. Science 292: 686–693.

Zheng, B., Y.L. Wang, C.C. Xia, D.Y. Huang, Y. Cao, J.S. Hao and C.D. Zhu. 2018. The complete mitochondrial genome of *Parnassius actius* (Lepidoptera: Papilionidae: Parnassinae) with the related phylogenetic analysis. Zool. Syst. 43: 1–17.

Zheng, B.X., Q.Q. Xu and Y.P. Shen. 2002. The relationship between climate change and Quaternary glacial cycles on the Qinghai-Tibetan Plateau: Review and speculation. Quat. Int. 97–98: 93–101.

Zhou, S.Z., X.L. Wang, J. Wang and L.B. Xu. 2006. A preliminary study on timing of the oldest Pleistocene glaciation in Qinghai-Tibetan Plateau. Quat. Int. 154–155: 44–51.

Zhu, R.W., Y.C. Li, D.L. Zhong and J.Q. Zhang. 2017. Establishment of the most comprehensive ITS2 barcode database to date of the traditional medicinal plant *Rhodiola* (Crassulaceae). Sci. Rep. 7: 10051.